The mass of β Pictoris c from β Pictoris b orbital motion

Lacour, S.; Wang, J.J.; Rodet, L.; Nowak, M.; Shangguan, J.; Beust, H.; ... ; Young, A.

Astronomy & Astrophysics manuscript no. BCmass
September 23, 2021

Letter to the Editor

The mass of β Pictoris c from β Pictoris b orbital motion

S. Lacour[1,2], J. J. Wang[3] ⋆, L. Rodet[4], M. Nowak[5], J. Shangguan[6], H. Beust[7], A.-M. Lagrange[7,1], R. Abuter[2], A. Amorim[8,9], R. Asensio-Torres[10], M. Benisty[7], J.-P. Berger[7], S. Blunt[3], A. Boccaletti[1], A. Bohn[11], M.-L. Bolzer[6], M. Bonnefoy[7], H. Bonnet[2], G. Bourdarot[6,7], W. Brandner[10], F. Cantalloube[12], P. Caselli[6], B. Charnay[1], G. Chauvin[7], E. Choquet[12], V. Christiaens[13], Y. Clénet[1], V. Coudé du Foresto[1], A. Cridland[11], R. Dembet[2], J. Dexter[14], P. T. de Zeeuw[11,6], A. Drescher[6], G. Duvert[7], A. Eckart[15,16], F. Eisenhauer[6], F. Gao[17], P. Garcia[9,18], R. Garcia Lopez[19,10], E. Gendron[1], R. Genzel[6], S. Gillessen[6], J. H. Girard[20], X. Haubois[21], G. Heißel[1], Th. Henning[10], S. Hinkley[22], S. Hippler[10], M. Horrobin[15], M. Houllé[12], Z. Hubert[7], L. Jocou[7], J. Kammerer[20], M. Keppler[10], P. Kervella[1], L. Kreidberg[10], V. Lapeyrère[1], J.-B. Le Bouquin[7], P. Léna[1], D. Lutz[6], A.-L. Maire[23,10], A. Mérand[2], P. Mollière[10], J. D. Monnier[24], D. Mouillet[7], E. Nasedkin[10], T. Ott[6], G. P. P. L. Otten[12,25], C. Paladini[21], T. Paumard[1], K. Perraut[7], G. Perrin[1], O. Pfuhl[2], E. Rickman[26], L. Pueyo[20], J. Rameau[7], G. Rousset[1], Z. Rustamkulov[20], M. Samland[27], T. Shimizu[6], D. Sing[20], J. Stadler[6], T. Stolker[11], O. Straub[6], C. Straubmeier[15], E. Sturm[6], L. J. Tacconi[6], E.F. van Dishoeck[11,6], A. Vigan[12], F. Vincent[1], S. D. von Fellenberg[6], K. Ward-Duong[28], F. Widmann[6], E. Wieprecht[6], E. Wiezorrek[6], J. Woillez[2], S. Yazici[6], A. Young[6], and the GRAVITY Collaboration

(Affiliations can be found after the references)

September 23, 2021

ABSTRACT

Aims. We aim to demonstrate that the presence and mass of an exoplanet can now be effectively derived from the astrometry of another exoplanet.
Methods. We combined previous astrometry of β Pictoris b with a new set of observations from the GRAVITY interferometer. The orbital motion of β Pictoris b is fit using Markov chain Monte Carlo simulations in Jacobi coordinates. The inner planet, β Pictoris c, was also reobserved at a separation of 96 mas, confirming the previous orbital estimations.
Results. From the astrometry of planet b only, we can (i) detect the presence of β Pictoris c and (ii) constrain its mass to $10.04^{+4.53}_{-3.10}\,M_{\rm Jup}$. If one adds the astrometry of β Pictoris c, the mass is narrowed down to $9.15^{+1.08}_{-1.06}\,M_{\rm Jup}$. The inclusion of radial velocity measurements does not affect the orbital parameters significantly, but it does slightly decrease the mass estimate to $8.89^{+0.75}_{-0.75}\,M_{\rm Jup}$. With a semimajor axis of 2.68 ± 0.02 au, a period of 1221 ± 15 days, and an eccentricity of 0.32 ± 0.02, the orbital parameters of β Pictoris c are now constrained as precisely as those of β Pictoris b. The orbital configuration is compatible with a high-order mean-motion resonance (7:1). The impact of the resonance on the planets' dynamics would then be negligible with respect to the secular perturbations, which might have played an important role in the eccentricity excitation of the outer planet.

Key words. Exoplanets – Astrometry and celestial mechanics – Instrumentation: interferometers – Techniques: high angular resolution

1. Introduction

The formation and evolution of giant exoplanets is an intense field of research. Several formation scenarios, ranging from gravitational instabilities (e.g., Boss 2011; Nayakshin 2017) to a variety of core-accretion models (e.g., Alibert et al. 2005; Emsenhuber et al. 2020), are still actively debated. The issue is the lack of observables with which to distinguish between the different scenarios. One solution is to analyze the atmospheric composition and search for formation signatures (Öberg et al. 2011; Mordasini et al. 2016; Madhusudhan et al. 2017). Another solution consists in measuring the energy dissipation during formation as a function of the final exoplanetary mass (Mordasini 2013; Marleau & Cumming 2014).

This paper focuses on the latter. Obtaining a dynamical mass for young directly imaged exoplanets is difficult. Only a handful of these objects have published dynamical masses: β Pictoris b (Snellen & Brown 2018; Dupuy et al. 2019; Lagrange et al. 2020; Vandal et al. 2020), β Pictoris c (Nowak et al. 2020), PDS 70 b (Wang et al. 2021), and HR8799 e (Brandt et al. 2021b). One of the main difficulties of a direct measurement is the long orbital period of directly imaged exoplanets. Another is the fact that young stars are often pulsating (for example, β Pictoris is a δ Scuti variable), which makes accurate radial velocity (RV) measurements difficult.

An efficient technique for measuring dynamical masses is observing multi-planetary systems and detecting the mutual influence of planets. The main historical example is the prediction of Neptune from the irregularities in the orbit of Uranus by Le Verrier (1846). A more recent example is the first exoplanetary system detected around PSR B1257+12 (Wolszczan & Frail 1992), where the mutual interactions of the planets were used to confirm their masses (e.g., Konacki & Wolszczan 2003). Last, transit timing variations (Agol et al. 2005) has become a key technique for obtaining the mass of transiting planets (e.g., Demory et al. 2020). In this paper we demonstrate that optical interferometry is now able to detect and measure the mass of an exoplanet solely from the astrometry of another exoplanet at larger separation.

⋆ 51 Pegasi b Fellow.

We focus on the β Pictoris system, where both the outer planet (b; Lagrange et al. 2010) and the inner planet (c; Lagrange et al. 2019) have well-characterized orbital parameters (Lagrange et al. 2020; Nowak et al. 2020). We use the GRAVITY instrument (Gravity Collaboration et al. 2017), a near-infrared interferometer operating at the Very Large Telescope (VLT) at Cerro Paranal. The interferometer has been designed to theoretically reach 10 μas accuracy (Lacour et al. 2014) and has effectively demonstrated this level of accuracy on SgrA* flares at the center of the Milky Way (Gravity Collaboration et al. 2018). On exoplanets, it has demonstrated a typical 50 μas accuracy (Gravity Collaboration et al. 2019; Lagrange et al. 2020).

In Sect. 2 we present the new data reduction and additional, recent astrometric observations. Section 3 presents the restricted three-body model that we use for the Markov chain Monte Carlo (MCMC) fits. In Sect. 4 β Pictoris c is detected from β Pictoris b astrometry only. In Sect. 5 we perform a fit that includes β Pictoris c astrometry and RVs. In Sect. 6 we discuss dynamical insights from the orbital solutions. Section 7 is the conclusion.

MJD (days)	ΔRA (mas)	ΔDEC (mas)	$\sigma_{\Delta RA}$ (mas)	$\sigma_{\Delta DEC}$ (mas)	ρ -
β Pictoris b					
58383.378	68.47	126.38	0.05	0.07	-0.86
58796.170	145.51	248.59	0.11	0.05	-0.85
58798.356	145.65	249.21	0.03	0.09	-0.44
58855.065	155.41	264.33	0.15	0.29	-0.71
58889.139	160.96	273.41	0.06	0.13	-0.56
59221.238	211.59	352.62	0.02	0.05	-0.10
59453.395	240.63	397.89	0.09	0.04	-0.91
β Pictoris c					
58889.140	-67.36	-112.59	0.17	0.24	-0.80
58891.065	-67.67	-113.20	0.11	0.19	-0.54
58916.043	-71.88	-119.60	0.07	0.14	-0.52
59220.163	–52.00	-80.86	0.20	0.34	-0.26

Table 1. Relative astrometry of β Pictoris c extracted from VLTI/GRAVITY observations. The Pearson coefficient (ρ) quantifies the correlation between the RA and Dec uncertainties.

2. Observations

We obtained three additional observations of the β Pictoris system with GRAVITY. Beta Pictoris c was observed during the night of 6 January 2021 and planet b during the nights of 7 January and 27 August 2021. The weather conditions ranged from very good to bellow average (on 27 January). The log of the observations are presented in Table A.1. These observations were part of the ExoGRAVITY large program (Lacour et al. 2020), taken with a similar observation sequence as for past exoplanet detections (Gravity Collaboration et al. 2019, 2020): The fringe tracker (Lacour et al. 2019) observes the star while the science camera (Straubmeier et al. 2014) alternately observes the star and the exoplanet.

The new observations of β Pictoris b and c were processed with the Public Release 1.5.0 (1 July 2021[1]) of the ESO GRAVITY pipeline (Lapeyrere et al. 2014). This new version has slightly better astrometric capabilities by accounting for the effect of differential astigmatism (GRAVITY Collaboration et al. 2021). We also reprocessed previously published GRAVITY data sets with the same pipeline version. From the seven epochs published by Lagrange et al. (2020), we discarded two data sets: one from 2 November 2019 and one taken on 7 January 2020. In both circumstances, the very low coherence time ($\tau_0 < 1.5$ ms) and limited number of exposures made the calculation of astrometric uncertainties difficult. The updated and new astrometric values are presented in Table 1.

3. A restricted three-body problem for multi-planetary systems

The Newtonian three-body problem is often addressed in a restricted version, where the mass of one body is negligible with respect to the other two (e.g., a satellite within the gravitational field of Earth and the Sun). Our case is different because the masses of the exoplanets are similar. However, a different restricted version of the three-body problem can be derived for systems with comparable masses. It uses Jacobi coordinates (Plummer 1918).

Beust (2003) already developed the formalism for any N-body system consisting of hierarchically nested orbits. Here we applied it to the specific case of a solar-mass object with two planets. The Lagrangian writes $L = T - V$, where T is the kinetic energy and V the potential energy. With three bodies interacting by gravitational force, this writes (G is the constant of gravitation):

$$L = \frac{1}{2}(m_\star \dot{\boldsymbol{x}}_\star^2 + m_b \dot{\boldsymbol{x}}_b^2 + m_c \dot{\boldsymbol{x}}_c^2) + \frac{G m_\star m_b}{|\boldsymbol{x}_b - \boldsymbol{x}_\star|} + \frac{G m_\star m_c}{|\boldsymbol{x}_c - \boldsymbol{x}_\star|} + \frac{G m_b m_c}{|\boldsymbol{x}_c - \boldsymbol{x}_b|}, \quad (1)$$

where $m_\star$ and $\boldsymbol{x}_\star$ correspond to the mass and position of the star, and m_b, $\boldsymbol{x}_b$, m_c, and $\boldsymbol{x}_c$, the mass and position of exoplanets b and c, respectively. To transform these equations into Jacobi coordinates, we set, according to Wisdom & Holman (1991):

$$\boldsymbol{q} = \boldsymbol{x}_c - \boldsymbol{x}_\star \quad (2)$$
$$\boldsymbol{Q} = \boldsymbol{x}_b - (m_\star \boldsymbol{x}_\star + m_c \boldsymbol{x}_c)\nu^{-1} \quad (3)$$
$$\boldsymbol{R} = (m_\star \boldsymbol{x}_\star + m_b \boldsymbol{x}_b + m_c \boldsymbol{x}_c)M^{-1}, \quad (4)$$

where $\boldsymbol{q}$ represents the position of planet c relative to the star, $\boldsymbol{Q}$ the position of planet b relative to the center of mass of the system (star, planet c), and $\boldsymbol{R}$ the position of the center of mass of the system. We also set $M = m_\star + m_b + m_c$ and $\nu = m_\star + m_c$.

The vectors $\boldsymbol{x}_{\star,b,c}$ can be rewritten in terms of these Jacobi coordinates:

$$\boldsymbol{x}_\star = \boldsymbol{R} - m_b M^{-1} \boldsymbol{Q} - m_c \nu^{-1} \boldsymbol{q} \quad (5)$$
$$\boldsymbol{x}_b = \boldsymbol{R} + (m_\star + m_b) M^{-1} \boldsymbol{Q} \quad (6)$$
$$\boldsymbol{x}_c = \boldsymbol{R} - m_b M^{-1} \boldsymbol{Q} + m_\star \nu^{-1} \boldsymbol{q}. \quad (7)$$

In the barycentric reference frame, where the velocity of the center of mass $\dot{\boldsymbol{R}}$ is zero, we have:

$$\dot{\boldsymbol{x}_\star} = -m_b M^{-1} \dot{\boldsymbol{Q}} - m_c \nu^{-1} \dot{\boldsymbol{q}} \quad (8)$$
$$\dot{\boldsymbol{x}_b} = (m_\star + m_b) M^{-1} \dot{\boldsymbol{Q}} \quad (9)$$
$$\dot{\boldsymbol{x}_c} = -m_b M^{-1} \dot{\boldsymbol{Q}} + m_\star \nu^{-1} \dot{\boldsymbol{q}} \quad (10)$$
$$\boldsymbol{x}_b - \boldsymbol{x}_\star = \boldsymbol{Q} + m_c \nu^{-1} \boldsymbol{q} \quad (11)$$
$$\boldsymbol{x}_c - \boldsymbol{x}_\star = \boldsymbol{q} \quad (12)$$
$$\boldsymbol{x}_c - \boldsymbol{x}_b = \boldsymbol{Q} - m_\star \nu^{-1} \boldsymbol{q}. \quad (13)$$

[1] https://www.eso.org/sci/software/pipelines/gravity/

The terms of Eq. (1) are replaced with these new expressions:

$$T = 1/2\left(m_c m_\star \nu^{-1}\dot{\boldsymbol{q}}^2 + m_b \nu M^{-1}\dot{\boldsymbol{Q}}^2\right) \quad (14)$$

$$V = -\frac{Gm_\star m_b}{\left|\boldsymbol{Q} + m_c\nu^{-1}\boldsymbol{q}\right|} - \frac{Gm_\star m_c}{|\boldsymbol{q}|} - \frac{Gm_b m_c}{\left|\boldsymbol{Q} - m_\star\nu^{-1}\boldsymbol{q}\right|}. \quad (15)$$

In the restricted case that matters to us ($|\boldsymbol{x_b} - \boldsymbol{x_\star}| >> |\boldsymbol{x_c} - \boldsymbol{x_\star}|$, i.e. $|\boldsymbol{Q}| >> |\boldsymbol{q}|$), the potential energy becomes, to first order:

$$V = -\frac{Gm_\star m_c}{|\boldsymbol{q}|} - \frac{Gm_b\nu}{|\boldsymbol{Q}|}, \quad (16)$$

and the Lagrangian can be approximated by:

$$L = \frac{1}{2}\left(m_c m_\star \nu^{-1}\dot{\boldsymbol{q}}^2 + m_b\nu M^{-1}\dot{\boldsymbol{Q}}^2\right) + \frac{Gm_\star m_c}{|\boldsymbol{q}|} + \frac{Gm_b\nu}{|\boldsymbol{Q}|}. \quad (17)$$

In this expression, the two Jacobi variables $\boldsymbol{Q}$ and $\boldsymbol{q}$ are decoupled, and the Lagrangian can be written as the sum of two terms, $L = L_q + L_Q$, with:

$$L_q = \frac{1}{2}\frac{m_c m_\star}{m_c + m_\star}\dot{\boldsymbol{q}}^2 + \frac{Gm_\star m_c}{|\boldsymbol{q}|} \quad (18)$$

$$L_Q = \frac{1}{2}\frac{m_b(m_\star + m_c)}{m_\star + m_b + m_c}\dot{\boldsymbol{Q}}^2 + \frac{Gm_b(m_\star + m_c)}{|\boldsymbol{Q}|}. \quad (19)$$

The term L_q corresponds to the Lagrangian of the classical two-body problem that describes the orbit of planet c around the star, whereas L_Q is the Lagrangian of the two-body problem corresponding to planet b orbiting around a virtual particle of mass $m_c + m_\star$ located at the center of mass of the system (star, planet c). Both quantities can be solved analytically. This is how we modeled the orbital motion of β Pictoris b and c. The model should be the same as that used in Brandt et al. (2021a). We validate that our orbital model is sufficiently accurate for our GRAVITY astrometry in Appendix B.

4. Detection of β Pic c "with the point of [a] pen"

Here, instead of a pen[2], we use the `orbitize!` code[3] (Blunt et al. 2020). In this section we fit the relative astrometry of β Pictoris b only to assess whether we can indirectly detect β Pictoris c. We fit both a one-planet model and a two-planet model to only the astrometry of β Pictoris b. The one-planet model is a repeat of the fit done in Gravity Collaboration et al. (2020), using the same eight orbital parameters: semimajor axis (a_b), eccentricity (e_b), inclination (i_b), argument of periastron (ω_b), position angle of the ascending node (Ω_b), epoch of periastron in fractional orbital periods after MJD 59,000 (τ_b), system parallax, and total mass ($M_{\rm tot}$). We used all the same priors as Gravity Collaboration et al. (2020). The two-planet model fit adds orbital elements for a second planet (a_c, e_c, i_c, ω_c, Ω_c, τ_c) as well as replacing total mass with component masses (M_* for the star and M_b and M_c for planets b and c, respectively). The priors on most of the orbital elements of β Pictoris c are the same as for b, except for a log uniform prior from 0.1 to 9 au for a_c. We used the same prior on $M_{\rm tot}$ as M_*. We used a log uniform prior of 1 to 50 $M_{\rm Jup}$ for M_c. We fixed the mass of M_b to 10 $M_{\rm Jup}$ since our orbital model described in Sect. 3 cannot particularly constrain M_b unless M_* is known to < 1% precision.

[2] Arago (1846) famously referred to Le Verrier's theoretical prediction of Neptune's existence as a discovery made with the point of his pen.
[3] `https://orbitize.readthedocs.io`

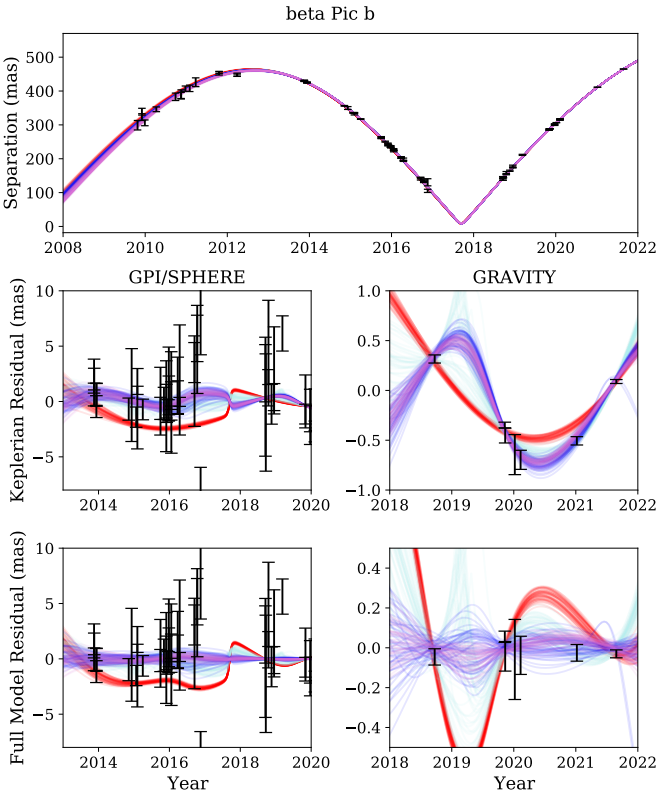

Fig. 1. Projected separation of β Pictoris b as a function of time. The one-planet and two-planet model fits that use only the b astrometry are shown in red and cyan, respectively. These models are described in Sect. 4. The two-planet model fit that uses b and c astrometry is also plotted, in blue, and the fit that also uses the RV is plotted in purple (Sect. 5). The top row shows the orbit models and all of the data. The middle row shows the residuals after subtracting a pure Keplerian orbit for planet b based on the orbital parameters from the two-planet model using b and c astrometry. The bottom row shows the residual after accounting for the perturbation of planet c. We note that, although the red one-planet model is a pure Keplerian orbit, it is not a flat line in the middle row because the best-fit one-planet Keplerian model also attempts to fit the perturbations due to the second planet.

In both cases we used the parallel-tempered affine-invariant sampler in `ptemcee` (Foreman-Mackey et al. 2013; Vousden et al. 2016), using 20 temperatures and 1000 walkers per temperature. We obtained 30,000 samples of the posterior per walker after a "burn-in" of 10,000 steps for each walker in the one-planet model fit. In the two-planet model fit, we obtained 5,000 samples of the posterior from each walker after a burn-in of 55,000 steps for each walker. The posteriors for the parameters are given in Table 2. For the one-planet fit, there are no assumptions – and therefore no constraints – on planet c. The two-planet fit is able to indirectly measure a distinct mass and a_c for the second planet.

To assess whether adding a second planet significantly improves the fit to the data, we computed the Bayesian information criterion (BIC) of the maximum likelihood model for both models. The one-planet model gives a BIC of 1247, while the two-planet model fit gives a BIC of 1784. The difference of 537 in the BIC indicates definitively that we have indirectly detected β Pictoris c using only the relative astrometry of β Pictoris b. For comparison, BIC changes between 10 and 100 have been used to show significant detections of outer planets in RV data (Christiansen et al. 2017; Bryan et al. 2019). This is also reflected in the residuals to the orbit fits shown in Fig. 1. In both the residuals to

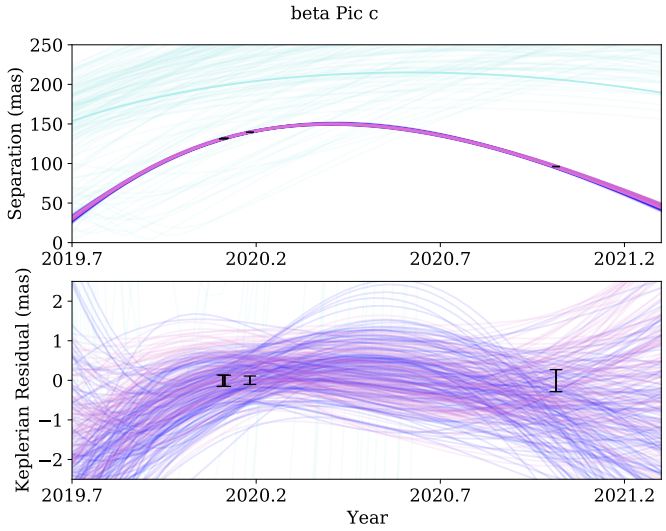

Fig. 2. Projected separation of β Pictoris c as a function of time. The top row shows the data (black error bars) and models (same coloring as Fig. 1). The bottom row shows the same data but after subtraction of the median orbit of the two-planet model fit from b and c astrometry. The two-planet model that uses only b astrometry (in teal) only weakly constraints the angular separation of planet c, and a direct detection of planet c is needed to obtain precise orbital constraints.

the GPI/SPHERE astrometry and the residual to the GRAVITY astrometry, the one-planet model fit in red fails to fully fit all of the data points and is systematically off. This corroborates the large change in BIC going from the one-planet to the two-planet model.

In addition to the detection of β Pictoris c, we also determined its mass, obtaining $10.04^{+4.53}_{-3.10}\,M_{\rm Jup}$. The estimate is slightly high, although it is still consistent with previous mass derivations (Lagrange et al. 2019; Vandal et al. 2020; Brandt et al. 2021a). The eccentricity was also determined, but with large uncertainties: $e_c = 0.90^{+0.08}_{-0.26}$. The value is high, although the 95% credible interval (in Table 2) is still consistent with previously published estimations. However, we have not included all of the data, and this merely demonstrates the ability of GRAVITY to indirectly detect a second planet in the system. The direct detection of β Pictoris c brings much better orbital constraints, as shown in the following section.

5. Refined masses and orbits of β Pic b and c

More accurate orbital parameters of β Pictoris c can be derived if we include the relative astrometry of c. This, in turn, gives a better mass estimation of c. The two-planet model fit was repeated, but with the addition of the β Pictoris c GRAVITY astrometry. The same MCMC walker parameters were used to obtain the 500,000 samples of the posterior. The posteriors are plotted in blue in both Fig. 1 (β Pictoris b) and Fig. 2 (β Pictoris c). The new β Pictoris c observation now accurately constrains the eccentricity of the orbit ($e = 0.32^{+0.03}_{-0.02}$) and the mass of β Pictoris c ($9.15^{+1.08}_{-1.06}\,M_{\rm Jup}$). The mass of β Pictoris c is consistent and comparable in precision to the mass obtained from stellar RVs and absolute astrometry (Lagrange et al. 2019; Vandal et al. 2020; Brandt et al. 2021a). This improves the robustness of the mass estimate since GRAVITY astrometry is not affected by systematic errors in stellar RVs on young stars or in absolute astrometry on bright stars.

Last, we performed a two-planet fit that included the RV data of the star from Lagrange et al. (2020) that was reprocessed by Vandal et al. (2020). The inclusion of the RV data allowed us to fit for the mass of β Pictoris b, which we had previously left fixed. We used a log uniform prior between 1 and 50 $M_{\rm Jup}$ for its mass prior. For the MCMC analysis, we used two temperatures and 1000 walkers per temperature. Each walker underwent a 10,000-step burn-in before 1,000 samples of the posterior were obtained from each walker. We find a semimajor axis of 2.68 ± 0.02 au, corresponding to an orbital period of 1221 ± 15 days. The mass estimate of β Pictoris c is still within the previous fit uncertainties, at $8.89^{+0.75}_{-0.75}\,M_{\rm Jup}$, and we estimate a mass of $11.90^{+2.93}_{-3.04}\,M_{\rm Jup}$ for β Pictoris b. Both component masses agree well with the latest dynamical mass estimates (Vandal et al. 2020; Brandt et al. 2021a). The two masses are also in very good agreement with a hot-core accretion scenario (Mordasini 2013), as proposed by Nowak et al. (2020).

6. Stability, resonance, and evaporating bodies

The β Pictoris system has only recently joined the selective group of multi-planet directly imaged systems, along with HR 8799 (Marois et al. 2008, 2010), PDS 70 (Keppler et al. 2018; Müller et al. 2018; Haffert et al. 2019), and TYC 8998-760-1 (Bohn et al. 2020). Because of the lack of planet detection and the struggle to constrain long-period orbits, the formation and dynamical evolution of cold giant planets remain largely unconstrained.

The eccentricity is thought to trace the formation and dynamical evolution of wide substellar objects. Indeed, wide-orbit giant planets and brown dwarfs appear to have different eccentricity distributions (Bowler et al. 2020). Low eccentricities and nearly planar planetary configurations are nevertheless usually associated with stable systems that formed via core accretion, such as the Solar System, even if post-formation giant impacts, planet-planet interactions, or scattering can excite orbital eccentricities afterward. With their orbits currently separated by ~ 5 relative Hill radii, the current configuration of the two planets is likely stable, a statement confirmed by Beust et al. (2021, in preparation). However, both planets presumably induce significant secular perturbations on each other due to their high masses. The eccentricity variations caused by these perturbations are detailed in Appendix C. It is interesting to note that, in most solutions from the orbital fit, planet b periodically reduces its eccentricity to a negligible value, while the eccentricity of planet c remains greater than 0.2. This suggests that, contrary to planet c, the eccentricity of planet b may not be primordial, but rather the result of secular perturbations from planet c. Secular interaction also applies to inclination. It has long been noted that the midplane of the inner disk differs from that of the outer (Mouillet et al. 1997; Heap et al. 2000; Augereau et al. 2001) by a few degrees. Secular perturbations arising from both planets themselves having inclination oscillations could indeed cause this phenomenon.

Both HR 8799 and PDS 70 planets are suspected to be in a configuration of mean-motion resonance (MMR; respectively $1:2:4:8$ and $2:1$; Wang et al. 2018, 2021). Although the orbital fits are not yet precise enough to confirm this, commensurable periods are compatible with the astrometric constraints and increase the stability of the systems. In the β Pictoris system, however, the separation between the planets forbids any low-order MMR. Figure 3 points to a possible $7:1$ configuration. Such a high-order MMR is not expected to have an impact on the dynamics of the planets, especially if we consider

		one-planet model	two-planet model	two-planet model	two-planet model
Parameter	Unit	b astrometry	b astrometry	b and c astrometry	RV + b and c astrometry
a_b	au	$10.01^{+0.02(+0.05)}_{-0.03(-0.05)}$	$10.01^{+0.03(+0.06)}_{-0.03(-0.06)}$	$9.95^{+0.03(+0.06)}_{-0.02(-0.05)}$	$9.93^{+0.03(+0.05)}_{-0.03(-0.05)}$
e_b		$0.104^{+0.003(+0.006)}_{-0.003(-0.006)}$	$0.110^{+0.004(+0.008)}_{-0.003(-0.007)}$	$0.106^{+0.004(+0.007)}_{-0.004(-0.007)}$	$0.103^{+0.003(+0.006)}_{-0.003(-0.005)}$
i_b	deg	$89.01^{+0.01(+0.02)}_{-0.01(-0.01)}$	$89.00^{+0.02(+0.04)}_{-0.04(-0.10)}$	$88.99^{+0.01(+0.02)}_{-0.01(-0.02)}$	$89.00^{+0.00(+0.01)}_{-0.01(-0.02)}$
ω_b	deg	$198.4^{+2.9(+5.5)}_{-3.1(-6.2)}$	$199.7^{+3.2(+6.3)}_{-3.5(-7.4)}$	$203.2^{+2.8(+5.2)}_{-3.2(-7.0)}$	$199.3^{+2.8(+4.9)}_{-3.1(-6.1)}$
Ω_b	deg	$31.79^{+0.01(+0.01)}_{-0.01(-0.02)}$	$31.90^{+0.03(+0.06)}_{-0.02(-0.05)}$	$31.80^{+0.00(+0.01)}_{-0.01(-0.02)}$	$31.79^{+0.01(+0.02)}_{+0.00(-0.01)}$
τ_b		$0.717^{+0.009(+0.018)}_{-0.009(-0.019)}$	$0.723^{+0.010(+0.019)}_{-0.011(-0.022)}$	$0.730^{+0.009(+0.017)}_{-0.010(-0.021)}$	$0.719^{+0.008(+0.014)}_{-0.010(-0.019)}$
a_c	au		$4.21^{+1.38(+3.43)}_{-1.33(-1.48)}$	$2.61^{+0.06(+0.12)}_{-0.06(-0.11)}$	$2.68^{+0.02(+0.05)}_{-0.02(-0.04)}$
e_c			$0.90^{+0.08(+0.10)}_{-0.26(-0.71)}$	$0.32^{+0.03(+0.06)}_{-0.02(-0.05)}$	$0.32^{+0.02(+0.03)}_{-0.02(-0.04)}$
i_c	deg		$90.52^{+10.81(+25.59)}_{-9.01(-26.24)}$	$88.92^{+0.10(+0.20)}_{-0.10(-0.20)}$	$88.95^{+0.09(+0.19)}_{-0.10(-0.20)}$
ω_c	deg		$27.1^{+20.4(+49.4)}_{-17.9(-25.7)}$	$60.8^{+4.2(+9.1)}_{-3.7(-7.0)}$	$66.0^{+1.8(+3.7)}_{-1.7(-3.7)}$
Ω_c	deg		$55.70^{+7.08(+15.14)}_{-6.74(-14.47)}$	$31.07^{+0.05(+0.10)}_{-0.04(-0.09)}$	$31.06^{+0.04(+0.08)}_{-0.04(-0.08)}$
τ_c			$0.804^{+0.080(+0.132)}_{-0.143(-0.189)}$	$0.708^{+0.012(+0.025)}_{-0.012(-0.023)}$	$0.724^{+0.006(+0.012)}_{-0.006(-0.013)}$
Parallax	mas	$51.44^{+0.12(+0.23)}_{-0.12(-0.24)}$	$51.44^{+0.12(+0.23)}_{-0.12(-0.24)}$	$51.44^{+0.12(+0.23)}_{-0.12(-0.24)}$	$51.44^{+0.12(+0.24)}_{-0.12(-0.24)}$
M_*	$M_\odot$		$1.75^{+0.02(+0.05)}_{-0.03(-0.05)}$	$1.73^{+0.03(+0.05)}_{-0.02(-0.04)}$	$1.75^{+0.03(+0.05)}_{-0.02(-0.04)}$
M_b	$M_{\rm Jup}$		10.00	10.00	$11.90^{+2.93(+5.68)}_{-3.04(-6.18)}$
M_c	$M_{\rm Jup}$		$10.04^{+4.53(+8.66)}_{-3.10(-4.32)}$	$9.15^{+1.08(+2.18)}_{-1.06(-2.11)}$	$8.89^{+0.75(+1.49)}_{-0.75(-1.47)}$

Table 2. Posteriors for the main parameters of the orbital fits. Orbital parameters are in Jacobi coordinates and follow the definitions in Blunt et al. (2020), with the exception of the reference epoch for τ as MJD 59,000 (31 May 2020). For each orbital parameter, the median is reported along with the 68% credible interval in super- and subscript (the 95% credible interval is reported in parentheses).

the high masses of the planets that will introduce non-negligible short-scale variations to the orbital elements.

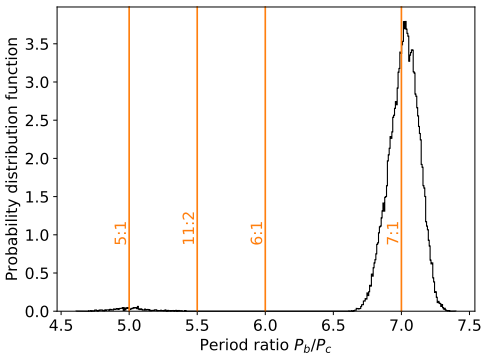

Fig. 3. Period ratio P_b/P_c distribution from the fit using all data (Sect. 5). If the system is in MMR, the most likely configuration would be the 7 : 1 commensurability.

The existence and characteristics of β Pictoris b had notably been postulated long before the first direct-imaging detection as a consequence of the observation of numerous falling evaporating bodies (FEBs) close to the star (Beust & Morbidelli 1996, 2000). Those star-grazing planetesimals were thought to come from an asteroid belt in 4 : 1 MMR with a slightly eccentric giant planet with predicted orbital characteristics that approximately match those of β Pictoris b (Thébault & Beust 2001; Beust & Valiron 2007). The presence of another massive planet such as β Pictoris c orbiting well inside β Pictoris b can perturb this picture. As a matter of fact, FEB progenitors trapped in 4:1 MMR with β Pictoris b (i.e., orbiting at ∼4 au from the star) undergo a gradual eccentricity increase with only little changes in semimajor axis before reaching the star-grazing state. This way they inevitably come to cross the orbit of β Pictoris c twice per orbit. Thus, close encounters with that planet would presumably eject most of the comets before they can become observable FEBs. Hopefully, the refined orbital and mass constraints provided in the present paper will help explore this rich dynamical issue. Beust et al. (2021, in preparation) show that the presence of β Pictoris c entirely prevents FEB progenitors from reaching the FEB state. Depending on its eccentricity, their source 4:1 MMR at 4 au may not even be stable. However, various inner MMRs with β Pictoris c (instead of b) could be a valuable alternate source of FEBs, leading to a revision of the FEB scenario.

7. Conclusions

Our results demonstrate the capabilities of relative astrometry with optical interferometry to characterize multi-planetary systems:

1. We were able to detect β Pictoris c and measure its mass from the astrometry of β Pictoris b alone. Our mass measurement of $10.04^{+4.53}_{-3.10}\,M_{\rm Jup}$ is in agreement with the previously published estimations based on RV by Lagrange et al. (2020) and Vandal et al. (2020). This is the first time that the presence of an exoplanet has been derived from the astrometry of another exoplanet.
2. The new detection of β Pictoris c, at 96 mas from its star, is a record in terms of exoplanet detection at small separation. Thanks to this new measurement, the orbital parameters of c, especially its eccentricity at 0.32 ± 0.02, are well determined. Fitting all data sets together, we obtain $8.89 \pm 0.75\,M_{\rm Jup}$ for β Pictoris c and $11.90^{+2.93}_{-3.04}\,M_{\rm Jup}$ for β Pictoris b.
3. Due to their masses and eccentricities, β Pictoris b and c are strongly interacting on secular timescales. The eccentricity of β Pictoris b may not be primordial but may simply be due to secular perturbations arising from β Pictoris c. The orbital parameters of the two planets point toward a possible 7 : 1 MMR.

Acknowledgements. Letter based on observations collected at the European Organisation for Astronomical Research in the Southern Hemisphere, ID 1104.C-0651. This research has made use of the Jean-Marie Mariotti Center `Aspro` service (`http://www.jmmc.fr/aspro`) . This research also made use of Astropy (`http://www.astropy.org`), a community-developed core Python package for Astronomy (The Astropy Collaboration et al. 2018). J.J.W. is supported by the Heising-Simons Foundation 51 Pegasi b Fellowship. The development of `orbitize!` is supported by the Heising-Simons Foundation through grant 2019-1698. We acknowledge support from the European Research Council under the Horizon 2020 Framework Program via the ERC grants 832428 (T.H.) and 757561 (A.V. and G.P.P.O.). A.A. and P.G. were supported by Fundação para a Ciência e a Tecnologia, with grants reference UIDB/00099/2020 and PTDC/FIS-AST/7002/2020.

Appendix A: Log of observations

The log of the three observations of β Pictoris system is presented in Table A.1.

Appendix B: N-body code versus Jacobi approximation

A corner plot of the key parameters obtained from the two-planet fit with b and c astrometry is shown in Fig. B.1.

To assess the validity of our orbit model for this two-planet fit with b and c astrometry, we used it to fit simulated astrometry of the β Pictoris system generated by an N-body integrator where we know the truth values. We used the `REBOUND` package with its IAS15 integrator to model the three-body system (Rein & Liu 2012; Rein & Spiegel 2015). We initialized the two planets at MJD 59,000 using the osculating orbital elements defined in the Truth column of Table B.1. We then integrated the planets forward and backward in time to simulate astrometry at every epoch where we have real astrometric data. For each epoch, random Gaussian noise was added to each measurement based on the corresponding reported measurement uncertainty at that epoch. We then estimated the orbital parameters with `orbitize!`, using the same procedure as above when fitting all of the astrometric data on both planets.

The median and 68% and 95% credible intervals are listed in Table B.1. The posteriors, as well as the truth values, are also plotted in Fig. B.2. We find that the orbital parameters and mass of β Pictoris c derived from the `orbitize!` model is accurate to within the 68% credible interval. The orbital elements of β Pictoris b sometimes appear beyond the 68% credible interval, indicating that the orbital model may have some biases in estimating the osculating orbital elements of planet b. Overall, we find the orbital model to be sufficiently accurate, especially for deriving a dynamical mass of β Pictoris c.

Appendix C: Secular evolution

Two planets orbiting a star mutually interact with each other. If they are in a stable configuration, their orbital elements will undergo variations on a timescale significantly larger than the orbital periods, the so-called secular variations. In a coplanar system (which we can consider β Pictoris to be), the evolution of the eccentricity can be derived analytically (Eq. 7.28 of Murray & Dermott 2000). For each solution of the orbital fits, we can then compute the period of the eccentricity oscillations and the range of eccentricities that the planets will reach within this period (see Fig. C.1).

References

Agol, E., Steffen, J., Sari, R., & Clarkson, W. 2005, Monthly Notices of the Royal Astronomical Society, 359, 567

Alibert, Y., Mordasini, C., Benz, W., & Winisdoerffer, C. 2005, Astronomy and Astrophysics, 434, 343

Arago, F. 1846, in Comptes rendus hebdomadaires des séances de l'Académie des sciences, Vol. 23 (Académie des sciences (France)), 659–662, https://gallica.bnf.fr/ark:/12148/bpt6k2980r/f663

Augereau, J. C., Nelson, R. P., Lagrange, A. M., Papaloizou, J. C. B., & Mouillet, D. 2001, A&A, 370, 447

Beust, H. 2003, Astronomy and Astrophysics, 400, 1129

Beust, H. & Morbidelli, A. 1996, Icarus, 120, 358

Beust, H. & Morbidelli, A. 2000, ıcarus, 143, 170

Beust, H. & Valiron, P. 2007, A&A, 466, 201

Blunt, S., Wang, J. J., Angelo, I., et al. 2020, AJ, 159, 89

Bohn, A. J., Kenworthy, M. A., Ginski, C., et al. 2020, ApJ, 898, L16

Boss, A. P. 2011, The Astrophysical Journal, 731, 74

Bowler, B. P., Blunt, S. C., & Nielsen, E. L. 2020, The Astronomical Journal, 159, 63

Brandt, G. M., Brandt, T. D., Dupuy, T. J., Li, Y., & Michalik, D. 2021a, AJ, 161, 179

Brandt, G. M., Brandt, T. D., Dupuy, T. J., Michalik, D., & Marleau, G.-D. 2021b, ApJ, 915, L16

Bryan, M. L., Knutson, H. A., Lee, E. J., et al. 2019, AJ, 157, 52

Christiansen, J. L., Vanderburg, A., Burt, J., et al. 2017, AJ, 154, 122

Demory, B. O., Pozuelos, F. J., Gómez Maqueo Chew, Y., et al. 2020, A&A, 642, A49

Dupuy, T. J., Brandt, T. D., Kratter, K. M., & Bowler, B. P. 2019, ApJ, 871, L4

Emsenhuber, A., Mordasini, C., Burn, R., et al. 2020, arXiv e-prints, 2007, arXiv:2007.05562

Foreman-Mackey, D., Hogg, D. W., Lang, D., & Goodman, J. 2013, Publications of the Astronomical Society of the Pacific, 125, 306

Gravity Collaboration, Abuter, R., Accardo, M., et al. 2017, Astronomy and Astrophysics, 602, A94

Gravity Collaboration, Abuter, R., Amorim, A., et al. 2018, Astronomy and Astrophysics, 618, L10

GRAVITY Collaboration, Abuter, R., Amorim, A., et al. 2021, A&A, 647, A59

Gravity Collaboration, Lacour, S., Nowak, M., et al. 2019, Astronomy and Astrophysics, 623, L11

Gravity Collaboration, Nowak, M., Lacour, S., et al. 2020, Astronomy and Astrophysics, 633, A110

Haffert, S. Y., Bohn, A. J., de Boer, J., et al. 2019, Nature Astronomy

Heap, S. R., Lindler, D. J., Lanz, T. M., et al. 2000, ApJ, 539, 435

Keppler, M., Benisty, M., Müller, A., et al. 2018, Astronomy and Astrophysics, 617, A44

Konacki, M. & Wolszczan, A. 2003, ApJ, 591, L147

Lacour, S., Dembet, R., Abuter, R., et al. 2019, A&A, 624, A99

Lacour, S., Eisenhauer, F., Gillessen, S., et al. 2014, Astronomy and Astrophysics, 567, A75

Lacour, S., Wang, J. J., Nowak, M., et al. 2020, in Society of Photo-Optical Instrumentation Engineers (SPIE) Conference Series, Vol. 11446, Society of Photo-Optical Instrumentation Engineers (SPIE) Conference Series, 114460O

Lagrange, A.-M., Bonnefoy, M., Chauvin, G., et al. 2010, Science, 329, 57

Lagrange, A.-M., Meunier, N., Rubini, P., et al. 2019, Nature Astronomy, 3, 1135

Lagrange, A. M., Rubini, P., Nowak, M., et al. 2020, A&A, 642, A18

Lapeyrere, V., Kervella, P., Lacour, S., et al. 2014, in Society of Photo-Optical Instrumentation Engineers (SPIE) Conference Series, Vol. 9146, Optical and Infrared Interferometry IV, ed. J. K. Rajagopal, M. J. Creech-Eakman, & F. Malbet, 91462D

Le Verrier, U.-J. 1846, in Comptes rendus hebdomadaires des séances de l'Académie des sciences, Vol. 23 (Académie des sciences (France)), 428–438, https://gallica.bnf.fr/ark:/12148/bpt6k2980r/f432

Madhusudhan, N., Bitsch, B., Johansen, A., & Eriksson, L. 2017, Monthly Notices of the Royal Astronomical Society, 469, 4102

Marleau, G.-D. & Cumming, A. 2014, Monthly Notices of the Royal Astronomical Society, 437, 1378

Marois, C., Macintosh, B., Barman, T., et al. 2008, Science, 322, 1348

Marois, C., Zuckerman, B., Konopacky, Q. M., Macintosh, B., & Barman, T. 2010, Nature, 468, 1080

Mordasini, C. 2013, A&A, 558, A113

Mordasini, C., van Boekel, R., Mollière, P., Henning, T., & Benneke, B. 2016, The Astrophysical Journal, 832, 41

Mouillet, D., Larwood, J. D., Papaloizou, J. C. B., & Lagrange, A. M. 1997, MNRAS, 292, 896

Müller, A., Keppler, M., Henning, T., et al. 2018, Astronomy and Astrophysics, 617, L2

Murray, C. D. & Dermott, S. F. 2000, Solar System Dynamics (Cambridge University Press)

Nayakshin, S. 2017, Publications of the Astronomical Society of Australia, 34, e002

Nowak, M., Lacour, S., Lagrange, A. M., et al. 2020, A&A, 642, L2

Öberg, K. I., Murray-Clay, R., & Bergin, E. A. 2011, The Astrophysical Journal Letters, 743, L16

Plummer, H. C. K. 1918, Cambridge

Rein, H. & Liu, S. F. 2012, A&A, 537, A128

Rein, H. & Spiegel, D. S. 2015, MNRAS, 446, 1424

Snellen, I. A. G. & Brown, A. G. A. 2018, Nature Astronomy, 2, 883

Straubmeier, C., Yazici, S., Wiest, M., et al. 2014, in Society of Photo-Optical Instrumentation Engineers (SPIE) Conference Series, Vol. 9146, Optical and Infrared Interferometry IV, ed. J. K. Rajagopal, M. J. Creech-Eakman, & F. Malbet, 914629

The Astropy Collaboration, Price-Whelan, A. M., Sipőcz, B. M., et al. 2018, AJ, 156, 123

Thébault, P. & Beust, H. 2001, A&A, 376, 621

Date	Target	UT Start Time	UT End Time	*N*exp / *N*DIT / DIT	airmass	τ_0	seeing
6 January 2021	β Pictoris c	02:32:52	04:01:17	18 / 32 / 10 s	1.12-1.18	7-13 ms	0.4-0.5"
7 January 2021	β Pictoris b	05:17:34	06:00:41	7 / 32 / 10 s	1.21-1.32	5-11 ms	0.4-0.7"
27 August 2021	β Pictoris b	09:00:31	09:46:39	5 / 16 / 30 s	1.24-1.39	2-3 ms	1.0-1.7"

Table A.1. Log of the two new GRAVITY observations. *N*exp is the number of exposures. *N*DIT and DIT are the number and duration of integrations per exposure. τ_0 is the coherence time.

Parameter	Truth	Fit Credible Interval
a_b	9.95	$9.90^{+0.03(+0.06)}_{-0.03(-0.06)}$
e_b	0.10	$0.09^{+0.01(+0.01)}_{+0.00(+0.00)}$
i_b	88.98	$89.00^{+0.01(+0.03)}_{-0.01(-0.02)}$
ω_b	202.05	$189.25^{+7.07(+10.96)}_{-7.15(-15.58)}$
Ω_b	31.81	$31.81^{+0.01(+0.02)}_{-0.01(-0.02)}$
τ_b	0.73	$0.69^{+0.02(+0.03)}_{-0.03(-0.05)}$
a_c	2.60	$2.55^{+0.90(+1.19)}_{-0.19(-0.27)}$
e_c	0.33	$0.37^{+0.05(+0.09)}_{-0.03(-0.06)}$
i_c	88.82	$88.83^{+0.19(+0.34)}_{-0.19(-0.38)}$
ω_c	61.02	$68.40^{+253.47(+257.53)}_{-11.18(-14.63)}$
Ω_c	31.06	$31.05^{+0.84(+1.06)}_{-0.07(-0.14)}$
τ_c	0.71	$0.71^{+0.14(+0.17)}_{-0.31(-0.32)}$
Parallax	51.39	$51.44^{+0.12(+0.24)}_{-0.12(-0.24)}$
M_b	10.00	10.00
M_c	8.85	$7.69^{+2.04(+4.32)}_{-3.42(-4.66)}$
M_*	1.75	$1.81^{+0.05(+0.09)}_{-0.04(-0.07)}$

Table B.1. Orbital parameters derived from fitting to simulated astrometry. The units are the same as in Table 2.

Vandal, T., Rameau, J., & Doyon, R. 2020, AJ, 160, 243

Vousden, W. D., Farr, W. M., & Mandel, I. 2016, Monthly Notices of the Royal Astronomical Society, 455, 1919

Wang, J. J., Graham, J. R., Dawson, R., et al. 2018, The Astronomical Journal, 156, 192

Wang, J. J., Vigan, A., Lacour, S., et al. 2021, The Astronomical Journal, 161, 148

Wisdom, J. & Holman, M. 1991, The Astronomical Journal, 102, 1528

Wolszczan, A. & Frail, D. A. 1992, Nature, 355, 145

[1] LESIA, Observatoire de Paris, PSL, CNRS, Sorbonne Université, Université de Paris, 5 place Janssen, 92195 Meudon, France
[2] European Southern Observatory, Karl-Schwarzschild-Straße 2, 85748 Garching, Germany
[3] Department of Astronomy, California Institute of Technology, Pasadena, CA 91125, USA
[4] Center for Astrophysics and Planetary Science, Department of Astronomy, Cornell University, Ithaca, NY 14853, USA
[5] Institute of Astronomy, University of Cambridge, Madingley Road, Cambridge CB3 0HA, United Kingdom
[6] Max Planck Institute for extraterrestrial Physics, Giessenbachstraße 1, 85748 Garching, Germany
[7] Université Grenoble Alpes, CNRS, IPAG, 38000 Grenoble, France
[8] Universidade de Lisboa - Faculdade de Ciências, Campo Grande, 1749-016 Lisboa, Portugal
[9] CENTRA - Centro de Astrofísica e Gravitação, IST, Universidade de Lisboa, 1049-001 Lisboa, Portugal
[10] Max Planck Institute for Astronomy, Königstuhl 17, 69117 Heidelberg, Germany
[11] Leiden Observatory, Leiden University, P.O. Box 9513, 2300 RA Leiden, The Netherlands
[12] Aix Marseille Univ, CNRS, CNES, LAM, Marseille, France
[13] School of Physics and Astronomy, Monash University, Clayton, VIC 3800, Melbourne, Australia
[14] JILA and Department of Astrophysical and Planetary Sciences, University of Colorado, Boulder, CO 80309, USA
[15] 1. Institute of Physics, University of Cologne, Zülpicher Straße 77, 50937 Cologne, Germany
[16] Max Planck Institute for Radio Astronomy, Auf dem Hügel 69, 53121 Bonn, Germany
[17] Hamburger Sternwarte, Universität Hamburg, Gojenbergsweg 112, 21029 Hamburg, Germany
[18] Universidade do Porto, Faculdade de Engenharia, Rua Dr. Roberto Frias, 4200-465 Porto, Portugal
[19] School of Physics, University College Dublin, Belfield, Dublin 4, Ireland
[20] Space Telescope Science Institute, Baltimore, MD 21218, USA
[21] European Southern Observatory, Casilla 19001, Santiago 19, Chile
[22] University of Exeter, Physics Building, Stocker Road, Exeter EX4 4QL, United Kingdom
[23] STAR Institute, Université de Liège, Allée du Six Août 19c, B-4000 Liège, Belgium
[24] Astronomy Department, University of Michigan, Ann Arbor, MI 48109 USA
[25] Academia Sinica Institute of Astronomy and Astrophysics, 11F Astronomy-Mathematics Building, NTU/AS campus, No. 1, Section 4, Roosevelt Rd., Taipei 10617, Taiwan
[26] European Space Agency (ESA), ESA Office, Space Telescope Science Institute, Baltimore, MD 21218, USA
[27] Department of Astronomy, Stockholm University, Stockholm, Sweden
[28] Five College Astronomy Department, Amherst College, Amherst, MA 01002, USA
[29] Research School of Astronomy & Astrophysics, Australian National University, ACT 2611, Australia

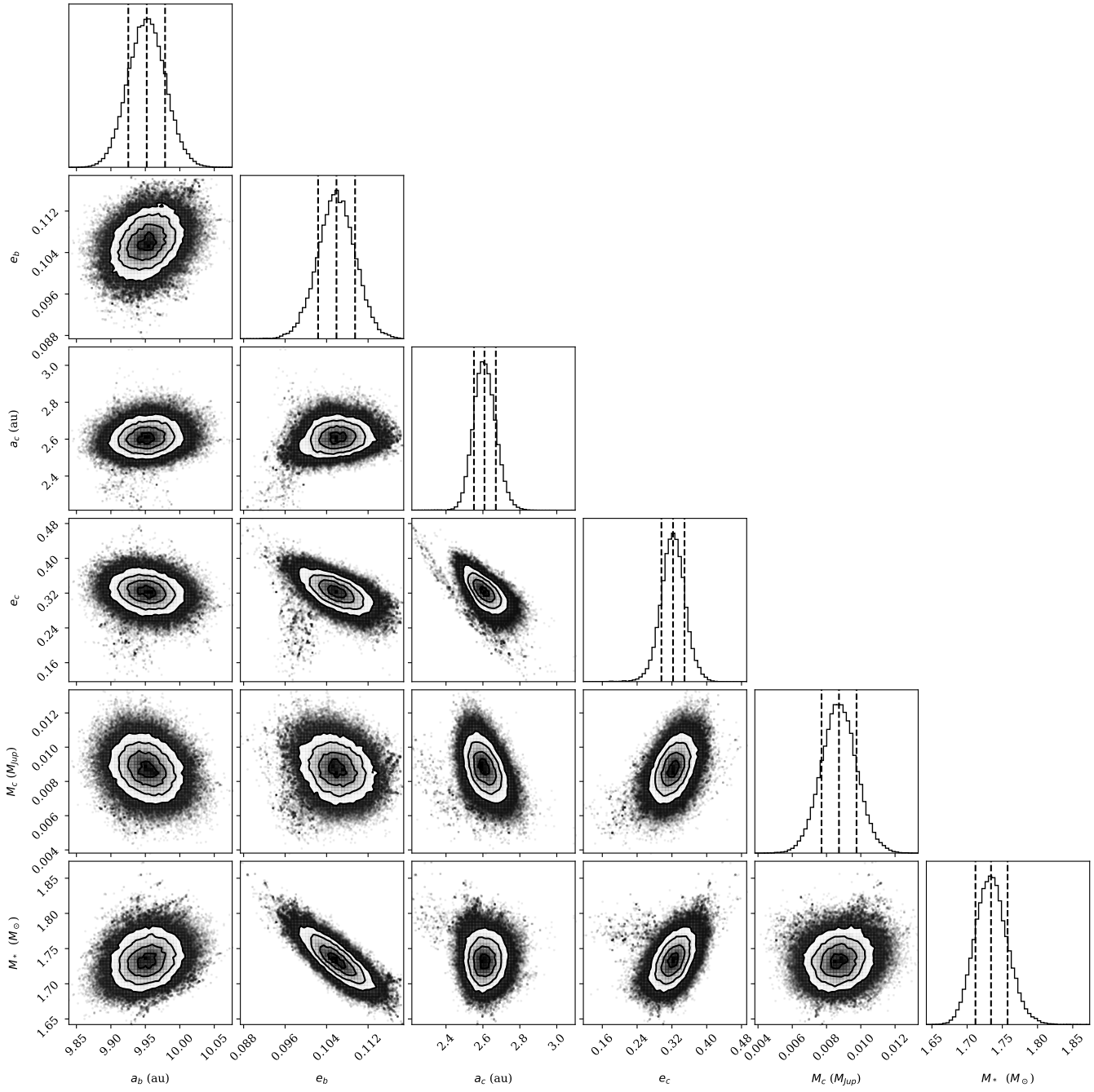

Fig. B.1. Corner plot of selected orbital parameters of interest for the two-planet model MCMC fit of the β Pictoris b astrometry only.

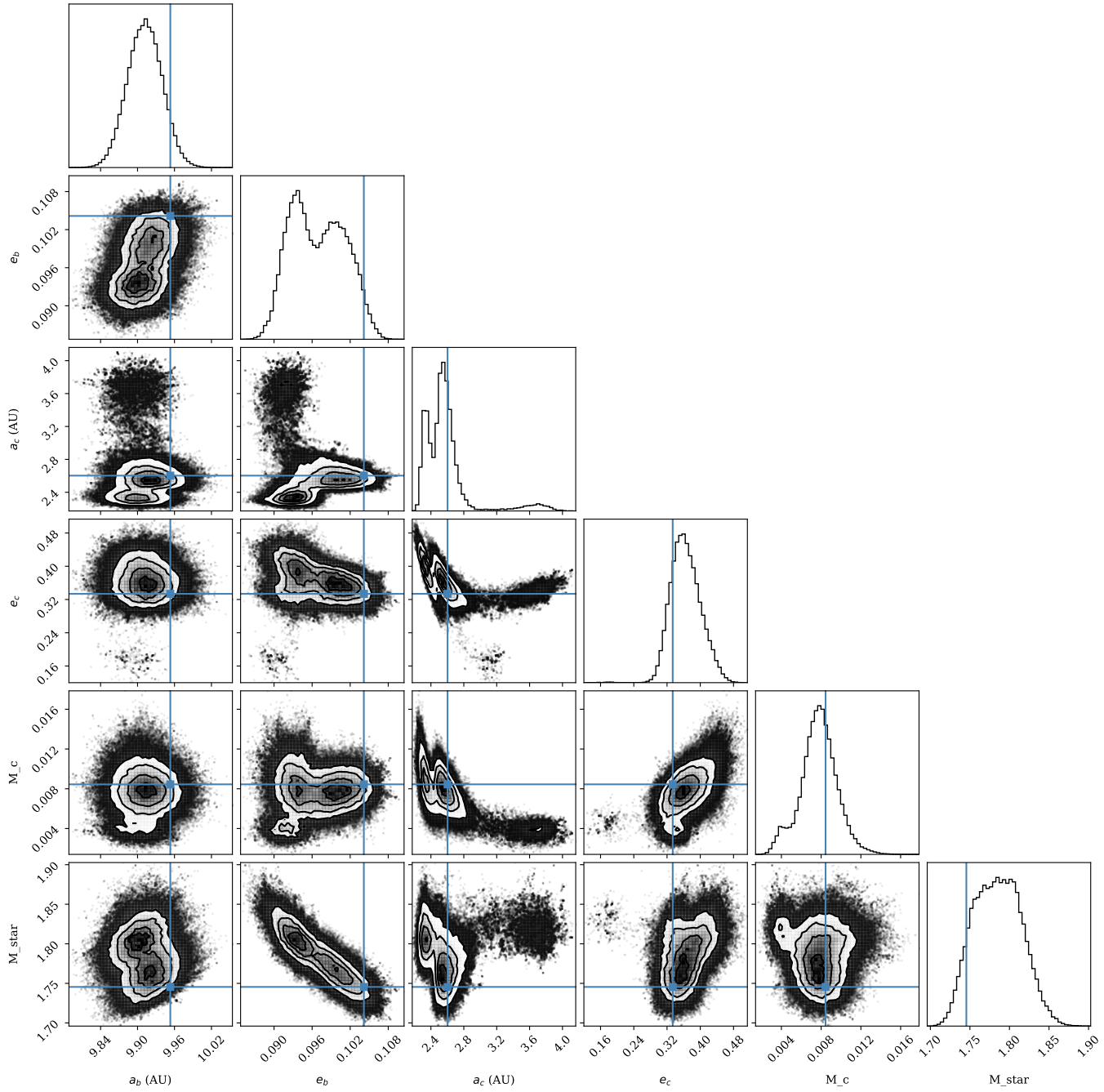

Fig. B.2. Corner plot of selected parameters of interest from the fit to simulated astrometry. Truth values of each parameter are plotted as cyan lines.

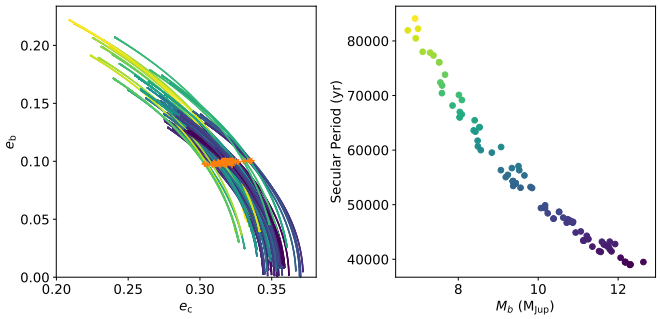

Fig. C.1. Secular evolution of the eccentricity of b and c due to their mutual interaction. Left is the trajectory in eccentricity phase space, starting from the observed values (orange crosses, which are random solutions to the orbital fit using all available data). The colors represent the corresponding eccentricity evolution period. The right panel represents the aforementioned period with respect to the mass of b.